Extreme Mechanics Letters 22 (2018) 89–97

Contents lists available at ScienceDirect

Extreme Mechanics Letters

journal homepage: www.elsevier.com/locate/eml

A facile, robust and versatile finite element implementation to study the time-dependent behaviors of responsive gels

Xu Wang [a], Zirui Zhai [a,b], Yuli Chen [b], Hanqing Jiang [a,*]

[a] School for Engineering of Matter, Transport and Energy, Arizona State University, Tempe, AZ 85287, USA
[b] Institute of Solid Mechanics, Beihang University (BUAA), Beijing, 100191, China

ARTICLE INFO

Article history:
Received 24 April 2018
Received in revised form 26 May 2018
Accepted 29 May 2018
Available online 5 June 2018

Keywords:
Gel
Transient
Finite element methods

ABSTRACT

Though there are significant efforts to develop numerical platforms to simulate the dynamic behaviors of responsive gels, several challenges were not successfully resolved, including truly robust method to handle time-dependent and coupled mass diffusion and deformation fields particularly at very short-time and complicated instability. In this Letter, a facile, robust and versatile finite element method was developed to resolve these challenges by adopting ramping boundary conditions, viscous damping, and damped Newton–Raphson method. This method can be readily implemented in a commercial platform COMSOL Multiphysics. The finite element method was showcased to study several dynamic examples that possess very short-time surface wrinkles, wrinkle evolutions, and incorporation with other physics field. Given the fact that the implementation is through a commercial platform, this method can have significant contributions to the studies of gels.

1. Introduction

Large and reversible deformation, responsiveness to various stimuli [1–7], and dual attributes of a solid and a liquid endow gels a wide variety of application [8–10]. Many theories have been formulated to describe the mass diffusion and deformation phenomenon in gels [11–22]. For example, nonlinear field theories have been developed to treat the fluid–solid mixture as a single homogenized continuum and rigorously consider the relationship between mass diffusion and large deformation. In addition to theoretical development, numerical implementation is another critical aspect to advance the frontier of gel related research. Many finite element-based methods have been developed, including in-house programs [23–25], several user-defined subroutines in the platform of ABAQUS (e.g., such as user-defined hyperelastic material [26–28]), user-defined element [29,30], user-defined heat transfer by an analogy between mass diffusion and heat transfer [31], and implementation through weak form PDE interface of COMSOL [32,33]. Despite these efforts, numerical implementation of nonlinear field theories for gels is still far from satisfactory. Firstly, in-house code is only limited to some specific problems and cannot be readily disseminated to the community [23–25]. Secondly, some user-defined subroutines can only capture the chemical equilibrium state [26–28]. Thirdly, even some implementations can study the time-dependent problems (i.e., dynamic or transient problems), very short-time transient behavior is still challenging due to the extremely inhomogeneous deformation [29–33]. Moreover, ubiquitous instability problems of gels during swelling/deswelling introduce another barricade for some implementations. Finally, to the best of our knowledge, no numerical implantation can robustly handle responsive gels that several physics fields coevolve, such as temperature sensitive gels. Consequently, a numerical implementation for gels with the following characteristics is desired: (1) robustness, i.e., the implementation can handle both time-dependent and equilibrium states and capture the evolution of various instability problems, (2) versatility, i.e., the method can study different responsiveness (e.g., heat) in gels, and (3) extensibility, i.e., the implementation can be readily extended to incorporate new fields with marginal efforts.

This letter reports a comprehensive finite element implementation of a nonlinear field theory for gels that possesses aforementioned three characteristics. Specifically, we implemented this method in COMSOL Multiphysics and adopted combined strategies to successfully handle the Dirichlet boundary conditions (i.e., prescribed chemical potential boundary conditions) for very short-time response, to efficiently configure the numerical solver for highly coupled problems (i.e., coupled mass diffusion and large deformation), and to effectively apply viscous damping for rich instability phenomena. Moreover, we can leverage the multiphysics capability of COMOSL to integrate with other physical fields. Finally, since this implementation is built on COMSOL Multiphysics

* Corresponding author.
E-mail address: hanqing.jiang@asu.edu (H. Jiang).

https://doi.org/10.1016/j.eml.2018.05.007
2352-4316/

via built-in functions or numerical servers, it can be readily disseminated to the community. In the paper, the numerical implementation will be introduced after a brief summary of the nonlinear field theory for gels. Then a wide spectrum of case studies will be presented to highlight the effectiveness and robustness of this implementation. Finally, this implementation will be extended to include co-evolution of three physical fields, namely, temperature, mass diffusion, and deformation, for thermoresponsive gels. It is believed that this finite element implementation can be readily applied to study time-dependent behaviors of responsive gels.

2. A brief review of a nonlinear field theory for gels

A nonlinear field theory for gels that couples large deformation and mass diffusion was developed by Hong et al. [18] using nominal variables, and was re-written by Duan et al. [31] using true variables in the current state in order to utilize the analogy between mass diffusion and heat transfer. Here the same formulation in Duan et al. [31] is adopted and the key equations are listed here. Deformation gradient $\mathbf{F} = \partial \mathbf{x}(\mathbf{X}, t)/\partial \mathbf{X}$ is used to map between the reference state (with coordinate $\mathbf{X}$) and the current state (with coordinate $\mathbf{x}(\mathbf{X}, t)$) and the standard mechanics equations are adopted. The gel is modeled as a hyperelastic material with normalized nominal free energy density $\hat{W}(\mathbf{F})$ given by

$$\begin{aligned}\hat{W}(\mathbf{F}, \mu) = & \frac{1}{2} N v \left[F_{iK} F_{iK} - 3 - 2 \log (\det \mathbf{F})\right] \\ & - \left[(\det \mathbf{F} - 1) \log \left(\frac{\det \mathbf{F}}{\det \mathbf{F} - 1}\right) + \frac{\chi}{\det \mathbf{F} - 1}\right] \\ & - \mu(\det \mathbf{F} - 1),\end{aligned} \tag{1}$$

where Nv and χ are two dimensionless materials properties representing the dimensionless shear modulus of the dry polymer and the enthalpy of mixing, respectively. μ is the chemical potential of the gel, with $\mu = -\infty$ for a dry polymer and $\mu = 0$ for a fully swollen or saturated gel. For diffusion, the conservation of mass can be expressed in terms of deformation gradient $\mathbf{F}$ given by

$$\frac{1}{\det \mathbf{F}} \frac{\partial \left[\det \mathbf{F} - 1\right]}{\partial t} + \frac{\partial \left[-\frac{[\det \mathbf{F} - 1] D}{\det \mathbf{F}} \frac{\partial \mu}{\partial x_i}\right]}{\partial x_i} = 0, \tag{2}$$

where t is time and D is the intrinsic diffusivity. The characteristic time scale τ_{ch} is given by $\frac{L^2}{D}$, where L is the feature size of the gel. Two types of boundary conditions can be prescribed for the mass diffusion, i.e., prescribed chemical potential boundary conditions $\mu = \overline{\mu}$ (i.e., Dirichlet boundary conditions), and prescribed flux boundary condition $\frac{\partial \mu}{\partial x_i} = \bar{j}_i$ (i.e., Neumann boundary conditions). Eqs. (1) and (2) co-evolve the deformation field (i.e., $\mathbf{F}$) and the chemical potential field (i.e., μ). The mechanical equilibrium was implemented in COMSOL Solid Mechanics module, and the hyperelastic material model of gel (Eq. (1)) was implemented using hyperelastic material node under Solid Mechanics module. The diffusion equation (Eq. (2)) was implemented via COMSOL PDE module. Linear elements have been used for both displacement and chemical potential field discretization [29] and they can be implemented directly by selecting shape function type and element order in COMSOL.

3. Finite element implementation of a robust and efficient method

Solving the coupled nonlinear field theories for gels is very challenging. To the best of our knowledge, a versatile and robust numerical platform that can handle both the short-time response of a gel, such as the transient response of a dry gel sobbed in a solvent, and the rich surface instability of the gel during the swelling/de-swelling processes, does not exist yet. At the short-time limit, the chemical potential of a dry gel experiences a sudden change, i.e., from $\mu = -\infty$ for the interior of the dry gel to $\mu = 0$ at the dry gel/solvent interfaces. Due to the large deformation of the gel, this sudden change of chemical potential at the vicinity of the gel/solvent interface will lead to extremely distorted deformation at the short-time limit, which attributes to the first challenge, namely, short-time response of a gel. If a representative diffusivity is considered, $D = 10^{-8}$ m^2/s, the characteristic time scale for a 1 mm^3 gel cube is 100 s. The reported shortest time scale for gel dynamic simulation is 215 s using a similar theory implemented by ABAQUS UEL, which did not capture the short-time surface wrinkling response and required significant coding. Another apparent challenge is the numerical convergence led by instability [26,27,34–37]. It should be pointed out that this instability does not only embody global buckling, but also can be local surface instability due to the materials properties [37]. For example, in the short-time period, swelling is usually accompanied by wrinkle formation, evolution and vanishing [35]. Therefore, slightly numerical perturbation can cause singularity of system matrix and lead to extreme numerical difficulty. To resolve aforementioned issues, three numerical strategies, namely ramping boundary conditions at the short-time limit, solver configuration for fully coupled problems, and viscous damping for numerical convergence at the presence of instability, will be adopted.

Ramping boundary conditions:

For a diffusion problem, at the prescribed chemical potential boundaries S_μ, a discontinuity exists at the gel and solvent interface. The extreme case for this discontinuity is for the dry gel where $\mu = \mu_{dry} = -\infty$ in the entire volume, except $\mu = \mu_{solvent} = 0$ at S_μ. Usually, this discontinuity will smear out with time and the chemical potential field will become smooth and infinitely differentiable [38]. However, for a strongly coupled mass diffusion and nonlinear large deformation problem, this discontinuity oftentimes leads to numerical divergence at the short-time limit. To tackle this problem, a smooth ramping boundary condition is introduced via a smoothed Heaviside function $H(t, t_{ramp})$ (Fig. 1a),

$$H(t, t_{ramp}) = \begin{cases} 0, t \le 0 \\ \text{ramping function}, \ 0 < t < t_{ramp} \\ 1, t \ge t_{ramp} \end{cases} \tag{3}$$

where a C^2 function (such as a high-order polynomial function) is introduced when $0 < t < t_{ramp}$, and thus the prescribed chemical potential is given by

$$\mu = \mu_{drygel} + (\mu_{solvent} - \mu_{drygel}) H(t, t_{ramp}). \tag{4}$$

The choice of the ramping function and t_{ramp} determines the smoothness of the prescribed chemical potential boundary conditions. The ramping boundary condition can be implemented via a built-in second derivative smooth Heaviside function flc2hs in COMSOL.

A benchmark test was performed to ensure an accurate representation of the discontinuous boundary condition using this ramping boundary condition. Over 10,000 linear hexahedral elements 8u8μ were used. Fig. 1b illustrates a gel bar with a unit length and lateral constrained in X_1 and X_2 directions. The gel only swells in the X_3 direction, characterized by the stretch $\lambda_3(X_3, t)$. The numerical benchmark solution of this 1D problem was given by Duan et al. [31]. From Fig. 1c–e, different ramping times t_{ramp}, ranging from $\frac{\tau_{ch}}{100}$, $\frac{\tau_{ch}}{10}$, and τ_{ch}, were studied, where $\tau_{ch} = \frac{L^2}{D}$ is the characteristic time. It can be seen that when $t_{ramp} = \frac{\tau_{ch}}{100}$, the finite element simulation agrees very well with the benchmark solution from very short time ($t = \tau_{ch}$), showing large inhomogeneous deformation, to longer time (Fig. 1c). Even with a larger ramping

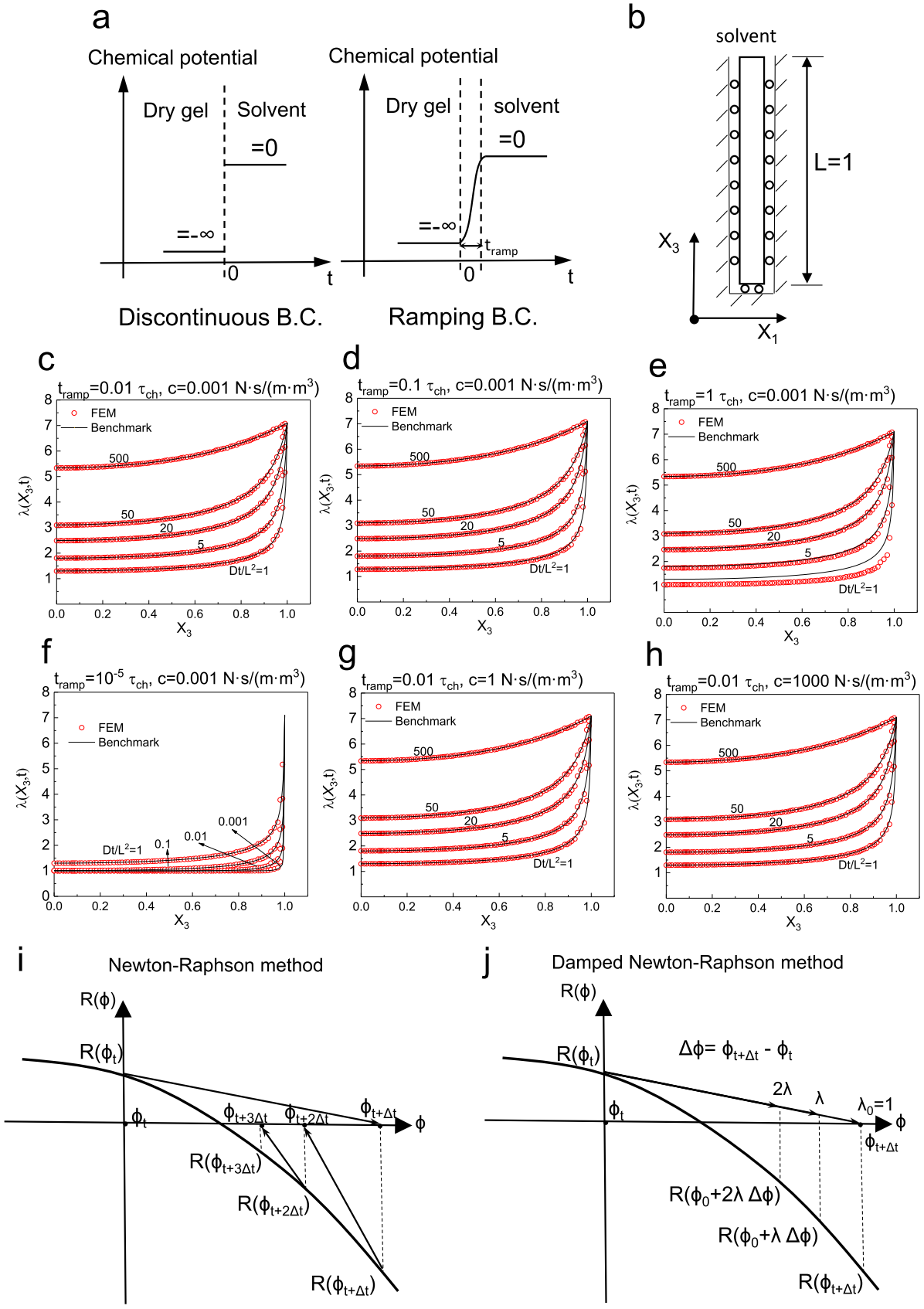

Fig. 1. Numerical methods to resolve the challenges to model transient behavior of gels. (a) Ramping boundary condition to resolve discontinuity at the interface between dry polymer and solvent. (b) Schematic of a gel swelling in X_3 direction. (c)–(h) Benchmark tests of a gel swelling in X_3 direction as compared with numerical benchmark solutions for $\left(t_{ramp} = \frac{\tau_{ch}}{100}, c = 0.001 \frac{\mathrm{N\,s}}{\mathrm{m\,m^3}}\right)$, $\left(t_{ramp} = \frac{\tau_{ch}}{10}, c = 0.001 \frac{\mathrm{N\,s}}{\mathrm{m\,m^3}}\right)$, and $\left(t_{ramp} = \tau_{ch}, c = 0.001 \frac{\mathrm{N\,s}}{\mathrm{m\,m^3}}\right)$, $\left(t_{ramp} = 10^{-5}\tau_{ch}, c = 0.001 \frac{\mathrm{N\,s}}{\mathrm{m\,m^3}}\right)$, $\left(t_{ramp} = 0.01\tau_{ch}, c = 1 \frac{\mathrm{N\,s}}{\mathrm{m\,m^3}}\right)$, and $\left(t_{ramp} = 0.01\tau_{ch}, c = 1000 \frac{\mathrm{N\,s}}{\mathrm{m\,m^3}}\right)$, respectively. (i) Newton–Raphson's method. (j) Damped Newton–Raphson's method.

time $t_{ramp} = \frac{\tau_{ch}}{10}$, the FEM solution still agrees perfectly with the benchmark solution (Fig. 1d). Only when the ramping time is comparable to the characteristic time, i.e., $t_{ramp} = \tau_{ch}$, the short-time limit from the FEM solution deviates from the benchmark solution, but the long-time solutions still match very well with the benchmark solutions (Fig. 1e). The benchmark tests show that as long as a proper ramping time is chosen (e.g. $t_{ramp} \sim \frac{\tau_{ch}}{10}$), the ramping boundary condition can accurately represent the discontinuous boundary conditions. In the present method, as long as the ramping time t_{ramp} is chosen to be short enough, very short time behavior can be captured. As shown in Fig. 1f, very short ramping time was used ($t_{\text{ramp}} = 1/10^5 \tau_{\text{ch}}$ which equals to $1/10^3$ s) and the present model can accurately capture the short time response $Dt/L^2 = 0.001$ (or $t = 0.1$ s). One thing should be kept in mind that high computational cost is expected in order to resolve very short time behavior (i.e., higher time resolution).

Viscous damping

The swelling and deswelling of many gels are accompanied by wrinkle formation, evolution and vanishing [35]. Traditional arc-length method is only suitable for problems with globally traceable load–displacement path [39] and not very efficient for gels with localized instabilities. Here a viscous damping method to tackle the instability issue in gel simulation was introduced.

For a global system matrix

$$\mathbf{K} = \begin{bmatrix} \mathbf{K^{uu}} & \mathbf{K^{u\mu}} \\ \mathbf{K^{\mu u}} & \mathbf{K^{\mu\mu}} \end{bmatrix}, \tag{5}$$

$\mathbf{K}^{uu}$ represents quasi-static solid mechanics physics, $\mathbf{K}^{u\mu}$ and $\mathbf{K}^{\mu u}$ are coupled time-dependent diffusion and deformation, and $\mathbf{K}^{\mu\mu}$ is the time-dependent diffusion. At the onset of instability, the global stiffness matrix $\mathbf{K}$ is singular because $\mathbf{K^{uu}}$ becomes singular. To solve this problem, a viscous damping factor c ($c > 0$) was introduced on $\mathbf{K^{uu}}$, which can be briefly explained as

$$\mathbf{K^{uu}}(\mathbf{u}) \cdot \mathbf{u} + c\frac{d\mathbf{u}}{dt} = \mathbf{P}(t) \tag{6}$$

and the modified equation is solved via an implicit method,

$$\mathbf{A}_{t+\Delta t} \Delta\mathbf{u} = \mathbf{Y}_{t+\Delta t} \tag{7}$$

with

$$\mathbf{A}_{t+\Delta t} = \frac{c}{\Delta t}\mathbf{I} + \mathbf{K}^{\mathbf{uu}}_{t+\Delta t}, \tag{8}$$

$$\mathbf{Y}_{t+\Delta t} = \mathbf{P}_{t+\Delta t} - c\frac{d\mathbf{u}_t}{dt} - \mathbf{K}^{\mathbf{uu}}_{t}\mathbf{u}_t, \tag{9}$$

where $\mathbf{I}$ is the identity matrix. By adjusting the positive number $\frac{c}{\Delta t}$, the modified stiffness matrix $\mathbf{A}_{t+\Delta t}$ can keep positive definite even at the onset of instability when $\mathbf{K}^{\mathbf{uu}}_{t+\Delta t}$ is singular. The physical meaning of the viscous damping term is an artificial friction to dissipate the energy. Thus, the choice of c is to ensure that the dissipated energy is just a small fraction of the total energy (e.g., 1% of the total energy). We studied the effect the magnitude of damping factor on the result. As it can be seen from Fig. 1c, g and h, damping factor varies from 10^{-3} N s/m^4 to10^3 N s/m^4 and does not have a strong influence on the computational results. This method can be implemented in COMSOL via spring foundation nodes on the solid domain. It is noted that the viscous damping method is similar to previous reported penalty factor method [30,31,39].

Solver configuration

Mass diffusion and large deformation concurrently evolve in gels. There are generally two approaches to solve coupled problems. One is a fully coupled approach that assembles both physics into one generalized stiffness matrix and applies Newton–Raphson method to solve until a convergence is reached. This approach generally requires a memory-intensive direct solver to solve the linear system in each Newton–Raphson iteration. The other approach is a segregated approach that solves each physics sequentially until convergence. This approach can usually be much more computationally efficient than the fully coupled approach. Unfortunately, the segregated method is not effective to model gels if not impossible, because of the strong coupling nature in gels. For gels, the deformation is extremely sensitive to chemical potential. Therefore, a slight change on chemical potential fields between two consecutive increments on solving the mass diffusion problem by fixing deformation fields may in turn lead to huge variations on the deformation fields on the next sequential solver for the displacement, which poses a significant challenge in convergence. Therefore, fully coupled solver has to be used to model the dynamics behavior of gels and a computationally efficient solver needs to be configured.

It is very computationally expensive to apply Newton–Raphson method for every iteration step, specifically for the fully coupled approach (Fig. 1i) where the inverse of the global residual matrix $\mathbf{R}(\boldsymbol{\phi}) = \mathbf{K}(\boldsymbol{\phi}) \cdot \boldsymbol{\phi} - \mathbf{P}$ is required to update the generalized nodal displacement $\boldsymbol{\phi}$ through

$$\boldsymbol{\phi}_{t+\Delta t} = \boldsymbol{\phi}_t + \boldsymbol{\Delta\phi} = \boldsymbol{\phi}_t - \mathbf{R}'\left(\boldsymbol{\phi}_t\right)^{-1} \cdot \mathbf{R}\left(\boldsymbol{\phi}_t\right). \tag{10}$$

To significantly reduce the computational cost, a damped Newton–Raphson iteration can be adopted [40] (Fig. 1j). Rather than directly compute $\boldsymbol{\phi}_{t+\Delta t}$ using Eq. (10), a damping factor $\lambda(\lambda \in [0, 1])$ is introduced so that

$$\boldsymbol{\phi}_{t+\Delta t} = \boldsymbol{\phi}_t + \lambda\boldsymbol{\Delta\phi} = \boldsymbol{\phi}_t - \lambda\mathbf{R}'\left(\boldsymbol{\phi}_t\right)^{-1} \cdot \mathbf{R}\left(\boldsymbol{\phi}_t\right). \tag{11}$$

The damping factor λ is adjusted based on the error $\mathbf{E}_t$, given by $\mathbf{R}'\left(\boldsymbol{\phi}_t\right)^{-1} \cdot \mathbf{E}_{t+\Delta t} = -\mathbf{R}\left(\boldsymbol{\phi}_{t+\Delta t}\right)$. If the relative error $|\mathbf{E}_{t+\Delta t}|$ is larger than the relative error $|\mathbf{E}_t|$ in the previous iteration, the damping factor λ will be reduced and $\boldsymbol{\phi}_{t+\Delta t}$ will be re-evaluated. The algorithm repeats the damping-factor reduction until the relative error is less than that in the previous iteration. When an acceptable $\boldsymbol{\phi}_{t+\Delta t}$ is achieved, the algorithm proceeds with the next damped Newton–Raphson iteration. This algorithm can significantly expedite the convergence speed for the fully coupled method. This algorithm has been implemented in COMSOL.

Case studies — dynamic and coupled mass diffusion and deformation

In this section, some dynamic behaviors of gels were studied to showcase the robustness of the finite element implementation. The cases with experimental results were chosen. Qualitative and quantitative comparisons were made.

Free swelling of a spherical gel

The free swelling of a spherical gel shows transition of surface wrinkles [35]. A spherical dry gel with initial radius of 1 mm was modeled, using over 20,000 tetrahedral elements. The materials properties used in this model are normalized dry gel modulus $Nv = 0.001$, diffusivity $D = 10^{-8}$ m^2/s, and enthalpy of mixing $\chi = 0.3$. The characteristic time τ_{ch} is 100 s and the ramping time $t_{ramp} = 0.5$ s. When immersing this spherical gel in water, the swelling of this gel shows evolution of the surface wrinkles as provided in Fig. 2, from very short time (e.g., $t = 0.4$ s or $t = 0.4\%\tau_{ch}$) to long time limit (e.g., $t = 30{,}000$ s). During the evolution, the characteristic wave length of wrinkles becomes larger and the number of wrinkles reduces, as wrinkles coalesce. Large inhomogeneous deformation was observed, particularly at the short time limit. At about 1000 s the gel reaches a perfect spherical again and continues to swell for thousands of seconds until reaches a final equilibrium state. The final radius of the spherical gel is 2.87 mm. Supplementary video S1 shows the pattern evolution. Similar patterns and kinetics of instability were

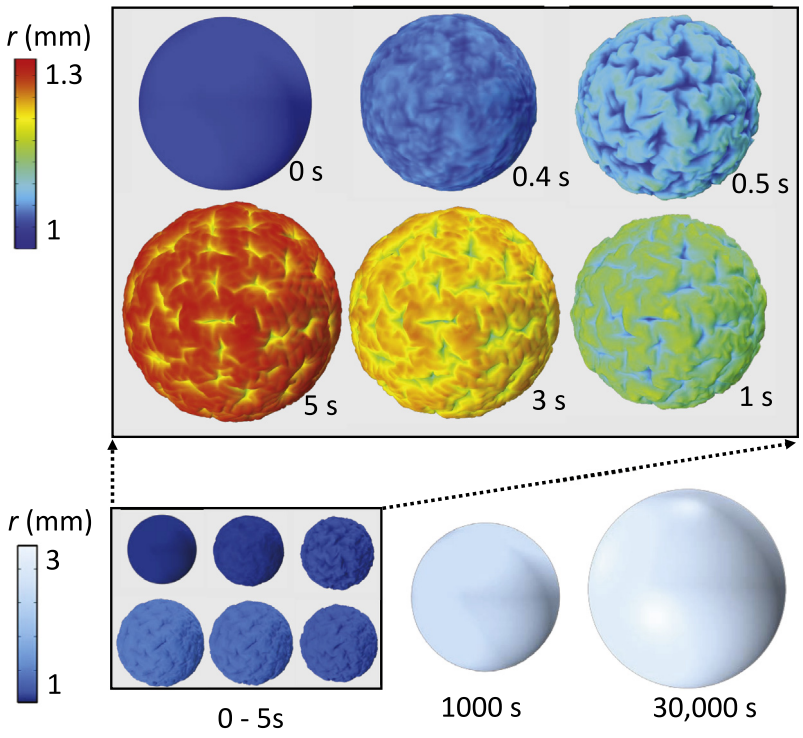

Fig. 2. Snapshots of a spherical gel free swelling at different time. Contour plots show the radius of the spherical gel at different time steps. The zoom-in contour plots highlight the short-time evolution of surface wrinkling when the dry polymer is sobbed in the solvent.

observed experimentally by Tanaka et al. [41] This study shows that the present finite element model can qualitatively capture the dynamic behavior of gels. We have checked the convergence and found that with increasing the number of elements, the lower-order modes have reached convergence, though the higher-order modes at very short time depend on the number of elements. The present method is also able to capture the evolution of creases as long as the surface self-contact does not appear. As shown in Fig. 2, the spherical gel shows both wrinkles and creases from 0.5 s to 5 s.

Constrained swelling of a gel strip

Another model to study the pattern formation of swelling gels is a soft gel bonded to a stiff substrate. The kinetics of this model is important for solving many biological problems, e.g., the development of embryos [42]. As shown in (Fig. 3a), characteristic dimensional parameters, h, t, and L represent height, thickness, and length of the strip in dry state, respectively. Depending on different dimensions of the strip gel, thousands of hexahedral elements were used in each case. The materials properties used in this model are normalized dry gel modulus $Nv = 0.001$, diffusivity $D = 10^{-7}$ m^2/s, and enthalpy of mixing $\chi = 0.57$. We found the evolution of the instability mode from local edge buckling into global buckling and the coalescence of sinusoidal buckling waves.

For a case with $t = 0.8$ mm, $h = 2$ mm and $L = 40$ mm, higher-order mode (i.e., local instability) appears at about 10 s (Fig. 3b for the top view and Fig. 3c for the 3D view), and then evolves to lower-order mode (i.e., global instability at about hundreds of seconds as shown in Fig. 3d). Two waves at 700 s marked with the arrows (Fig. 3d) coalesce into one big wave at 1200 s (Fig. 3e). After another coalescence between 1200 s and 30,000 s marked by two arrows, the striped gel reaches equilibrium state (Fig. 3f for the top view and Fig. 3g for the 3D view). The dynamic of wave evolution is provided in the supplementary video S2 (top view). Both the evolution of the instability mode and the coalescence of waves were observed experimentally by DuPont et al. [43].

We also studied the relationship between wavelength λ and height h at equilibrium state. In order to compare with the theoretical model for a strip with infinite length [44], the length L in the numerical simulation was make much larger than the height h. Specifically, $L = 100$ mm was used for all simulations, and h varied from 1 mm to 6 mm. In three groups of samples with different normalized thickness t/h, the ratio of λ to h approximately falls in the range of the theoretical model when $\lambda/h = 3.256$ (Fig. 3h). The discrepancy can be resulted from the fact that the theoretical model is based on linear elasticity while this work is based on nonlinear theory [44].

Gel tube swelling

Another constrained swelling case is a gel tube on a stiff substrate. The gel tube in dry state can be described by three characteristic dimensional parameters, t, h, and d, representing thickness, height, and diameter (Fig. 4a), respectively. The same material parameters as that in the strip gel were used. Depending on different dimensions of the gel tube, thousands of linear hexahedral elements 8u8μ were used in each case. Subjected to a fixed boundary condition on the bottom, the gel develops inhomogeneous stress when contacts with the solvent. In the case with $t/h = 0.5$ and $h/d = 0.14$, the phenomenon of wave coalescence can be observed. The tubular gel buckles into seven waves at 42 s, with two of the waves pointed by arrows (Fig. 4b). Then at 50 s the two marked waves coalesce into one wave (Fig. 4c), which is much larger than other waves. At 600 s all the six waves are in equal size and the gel reaches its equilibrium state (Fig. 4d). Supplementary video S3 shows the dynamic evolution. We also studied the effect of gel tube geometry on wrinkle patterns. Three groups of simulations with different normalized thickness t/h and each group having seven cases with different normalized height h/d were performed. The configurations of all the cases at their equilibrium states are shown in Fig. 4e. As shown in Fig. 4f, the relationship between the number of waves at the equilibrium state

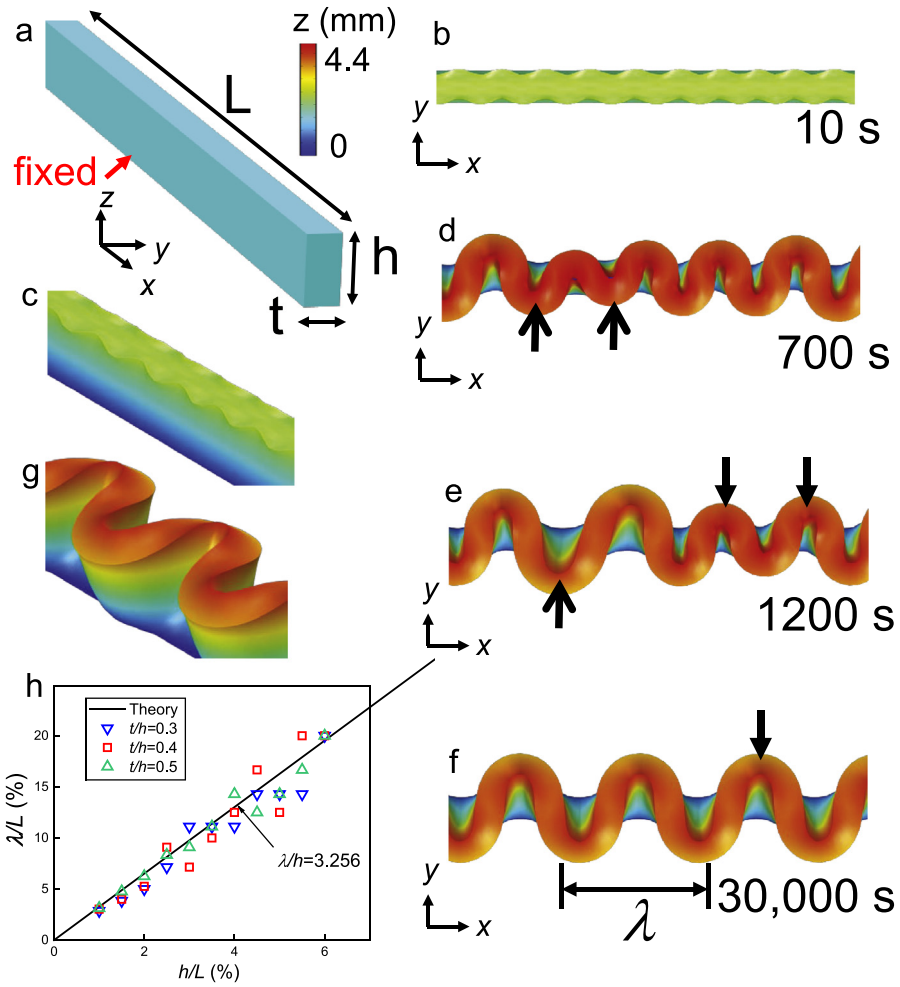

Fig. 3. Gel strip constrained swelling. (a) Schematic of gel strip with bottom surface fixed. (b)–(g) Snapshots of gel strip constrained swelling and the contour plots are for the z coordinate. (b) Top view of the gel at time 10 s, showing higher-order local instability. (c) Side view of Fig. 3b. (d) Top view of the gel at time 700 s, showing global instability mode. Two waves are marked by arrows. (e) Top view of the gel at time 1200 s, where buckling waves coalesce from Fig. 3d. (f) Top view of the gel at time 30,000 s (close to the equilibrium state), where buckling wave coalesce is shown. (g) Side view of Fig. 3f. (h) Normalized instability wavelength λ/L as a function of the normalized height h/L of the swollen gel strips at different thickness to height ratios (t/h) compared with theoretical results.

and the normalized height h/d matches well with the theory of Lee et al. [45].

Bifurcation of a lattice of cylindrical holes

A gel stab with a square lattice of through cylindrical holes swells in a solvent. As shown in Fig. 5, following the work of Hong et al. [28], we model a unit cell containing quarters of four neighboring holes using plane-strain elements [28]. Over 10,000 linear quadrilateral elements 4u4μ were used. Here, we can capture the entire time-dependent snap-through bifurcation process, which was believed to be very difficult in ABAQUS for this type of problem [28]. The evolution of the chemical potential is plotted on the deformed layer at different time. As solvent molecules migrate into the gel, the field of chemical potential μ gradually diffuses from boundaries into centers of the gel. At the same time, cylindrical holes collapse into slits, and the square lattice bifurcates into slits of alternating directions with symmetry broken. The materials properties used in this model are $N\nu = 0.001, D = 10^{-8}\,\mathrm{m^2\,s^{-1}}$ and $\chi = 0.85$. Supplementary video S4 shows the dynamic evolution.

Case study – coupled heat transfer, mass diffusion and large deformation for thermoresponsive gels

The method developed in this paper can be readily extended to incorporate other physics. Here we showcase the versatility of this method by modeling the transient process of a thermoresponsive gel. The fully swollen thermoresponsive gel PNIPAM is in a hemispherical shell shape [46]. To trigger the localized deswelling by increasing temperature, Joule heating was utilized via three fan-shaped heaters (I, II and III) embedded in the shell (Fig. 6a), which can be turned on/off by controlling the current passing through them. The equilibrium state, both thermal and mechanical fields, were studied separately [46]. In this section, the transient process that captures the time-dependent evolution of temperature, diffusion, and deformation fields, was studied. The model parameters are the followings. The inner and outer radius of the hemispherical shell are 7 mm and 8 mm, respectively. The bottom of the shell is fixed to constrain rigid body movement, and all outer surface are subjected to convective heat transfer with coefficient taken to be $h = 200\ \mathrm{W\,m^{-2}\,K^{-1}}$ [47]. The current is 44 mA and the resistance of each heater is 126 Ω. The materials properties used in this model are normalized dry gel modulus $N\nu = 0.001$ and diffusivity $D = 10^{-8}\ \mathrm{m^2\,s^{-1}}$. The coupling between mass diffusion and temperature is characterized by a temperature dependent enthalpy of mixing $\chi(T)$, i.e., the lower critical solution temperature phenomena of PNIPAM gels [46]. The thermal field evolves based on the conservation of heat in heat transfer,

$$\rho C_p \frac{\partial T}{\partial t} + \nabla\,(-k\nabla T) = 0, \tag{12}$$

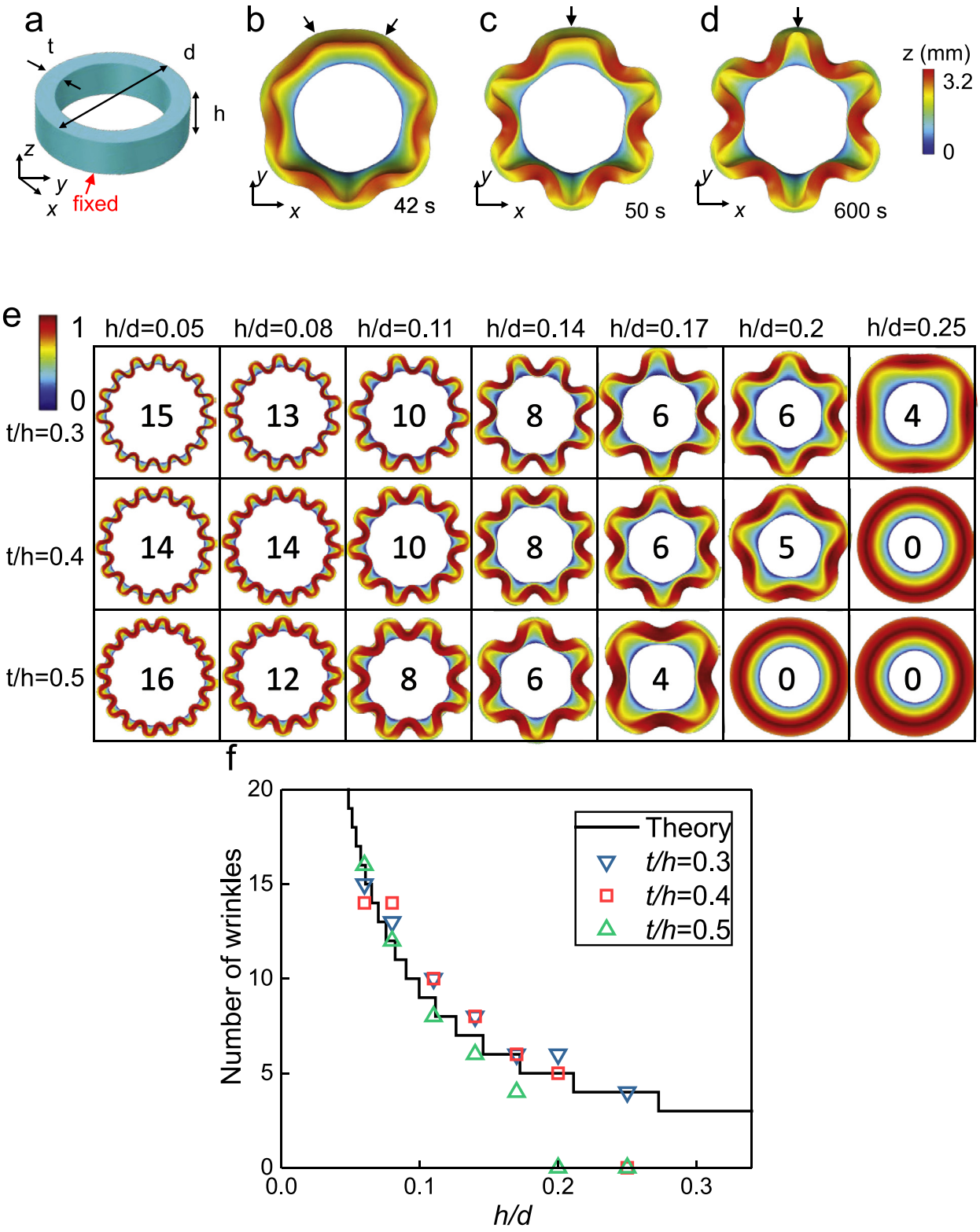

Fig. 4. Gel tube constrained swelling. (a) Schematic of gel tube with bottom surface fixed. (b)–(d) Snapshots of gel tube constrained swelling and the contour plots are for the z coordinate. (b) Top view of the gel at time 42 s, where two arrows mark two buckling peaks. (c) Top view of the gel at time 50 s, where two buckling peaks in Fig. 4b coalesce into one peak. (d) Top view of the gel at time 600 s (close to the equilibrium state). (e) A combination of equilibrium shapes with different height to diameter (h/d) and thickness to height (t/h) ratios. The contour plots are for the z coordinate. (f) Number of wrinkles along the circumferential direction as a function of h/d with different t/h compared with theoretical results.

where ρ, C_p, and k are the density, specific heat capacity and thermal conductivity of the gel, respectively. Given that gel is a mixture of water and polymer, rule of mixture was used to assign these material properties. Moreover, the amount of water in a gel depends on deformation and so does these material properties. For example, the specific heat capacity of gel is given by

$$C_p(\mathbf{F}) = \frac{1}{\det \mathbf{F}}(C_p)_{\text{dry gel}} + (1 - \frac{1}{\det \mathbf{F}})(C_p)_{\text{water}}, \tag{13}$$

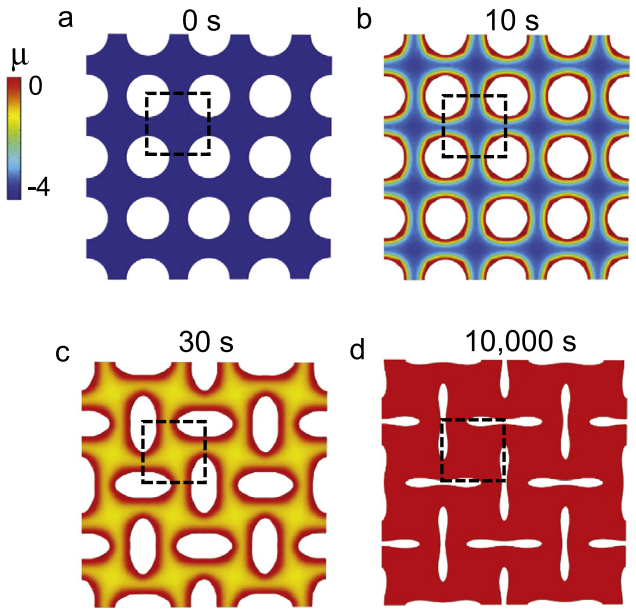

Fig. 5. Swelling of a gel stab with a pattern of cylindrical holes. The contour plots are for the chemical potential at the deformed states at different time, with (a) for the initial state, (b) for 10 s, (c) for 30 s, and (d) for 10,000 s.

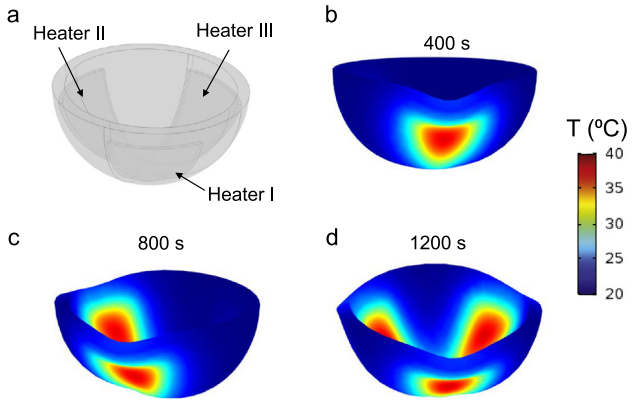

Fig. 6. Dynamic response of a hemispherical thermoresponsive hydrogel. (a) Schematic of the hemispherical hydrogel shell made of PNIPAM embedded with three heaters. The contour plots are for the temperature field at the deformed states at different time, with (a) for 400 s where only heater I is ON, (b) for 800 s where both heaters I and II are ON, and (c) for 1200 s where all heaters are ON.

where $(C_p)_{\text{water}} = 4187\ \text{J kg}^{-1}\ \text{K}^{-1}$ and $(C_p)_{\text{dry gel}} = 1500\ \text{J kg}^{-1}\ \text{K}^{-1}$. Because the density and conductivity of water and dry gel are close [48], it is not necessary to differentiate water and dry gel for these two properties in our case.

In the simulation, over 10,000 linear tetrahedral elements 4u4μ4T were used. We turn on heater I first, and then turn on heaters II and III in sequence with a time gap of 400 s. The contour plots in Fig. 5b–d show the temperature field. It can be seen from Fig. 5b at 400 s that the deswelling of Section 1 yields identical shape as that in the experiment [46]. After 800 s as shown in Fig. 5c, the deswelling of Sections 1 and 2 again lead to two localized deformation patterns, which is the same as that reported in the experiments. Finally at 1200 s, all heaters have been turned on for at least 400 s, and the deswellon pattern reproduces the experimental observations. The dynamic evolution is clearly shown in the supplementary video S5. This case demonstrates the versatility of this method.

4. Conclusion

In this paper, a robust and versatile finite element implementation has been developed to study the dynamic response of responsive gels that have coupled mass diffusion and deformation fields, and other physics fields. Ramping boundary conditions were adopted to resolve the numerical challenge for very short-time limit where the chemical potential has a discontinuity. Viscous damping was introduced to robustly simulate instability and damped Newton–Raphson method was used to more efficiently solve a fully coupled problem. Since this method can be readily implemented in COMSOL Multiphysics by entering Eqs. (1) and (2) in Solid Mechanics and PDE modules, respectively, other physics fields can be incorporated with minimum efforts. This method and implementation provide unprecedented capability to model the dynamic response of responsive gels. Given the fact that the implementation is through a commercial platform, this method can have significant contributions to the studies of gels.

Acknowledgments

The work at ASU is financially support by the National Science Foundation CMMI 1462481. The work at Beihang is supported by the National Natural Science Foundation of China (Nos. 11622214 and 11472027).

Appendix A. Supplementary data

Supplementary material related to this article can be found online at https://doi.org/10.1016/j.eml.2018.05.007.

Supplementary Materials contains 5 supplementary videos.

References

[1] J. Gong, T. Nitta, Y. Osada, Electrokinetic modeling of the contractile phenomena of polyelectrolyte gels. One-dimensional capillary model, J. Phys. Chem. 98 (1994) 9583–9587.
[2] R. Luo, H. Li, K.Y. Lam, Modeling and simulation of chemo-electro-mechanical behavior of pH-electric-sensitive hydrogel, Anal. Bioanal. Chem. 389 (2007) 863–873.
[3] A. Richter, et al., Review on hydrogel-based pH sensors and microsensors, Sensors 8 (2008) 561–581.
[4] A. Suzuki, T. Ishii, Y. Maruyama, Optical switching in polymer gels, J. Appl. Phys. 80 (1996) 131–136.
[5] A. Suzuki, T. Tanaka, Phase transition in polymer gels induced by visible light, Nature 346 (1990) 345.
[6] T. Tanaka, I. Nishio, S.-T. Sun, S. Ueno-Nishio, Collapse of gels in an electric field, Science 218 (1982) 467–469.
[7] T. Wallmersperger, D. Ballhause, B. Kröplin, M. Günther, G. Gerlach, Coupled multi-field formulation in space and time for the simulation of intelligent hydrogels, J. Intell. Mater. Syst. Struct. 20 (2009) 1483–1492.
[8] P. Bawa, V. Pillay, Y.E. Choonara, L.C. Du Toit, Stimuli-responsive polymers and their applications in drug delivery, Biomed. Mater. 4 (2009) 022001.
[9] T. Miyata, T. Uragami, K. Nakamae, Biomolecule-sensitive hydrogels, Adv. Drug Delivery Rev. 54 (2002) 79–98.
[10] Y. Qiu, K. Park, Environment-sensitive hydrogels for drug delivery, Adv. Drug Delivery Rev. 53 (2001) 321–339.
[11] N. Bouklas, R. Huang, Swelling kinetics of polymer gels: comparison of linear and nonlinear theories, Soft Matter 8 (2012) 8194–8203.
[12] S. Cai, Z. Suo, Mechanics and chemical thermodynamics of phase transition in temperature-sensitive hydrogels, J. Mech. Phys. Solids 59 (2011) 2259–2278.
[13] S.A. Chester, A constitutive model for coupled fluid permeation and large viscoelastic deformation in polymeric gels, Soft Matter 8 (2012) 8223–8233.
[14] S.A. Chester, L. Anand, A coupled theory of fluid permeation and large deformations for elastomeric materials, J. Mech. Phys. Solids 58 (2010) 1879–1906.
[15] S.A. Chester, L. Anand, A thermo-mechanically coupled theory for fluid permeation in elastomeric materials: application to thermally responsive gels, J. Mech. Phys. Solids 59 (2011) 1978–2006.
[16] F.P. Duda, A.C. Souza, E. Fried, A theory for species migration in a finitely strained solid with application to polymer network swelling, J. Mech. Phys. Solids 58 (2010) 515–529.
[17] W. Hong, X. Zhao, Z. Suo, Large deformation and electrochemistry of polyelectrolyte gels, J. Mech. Phys. Solids 58 (2010) 558–577.

[18] W. Hong, X. Zhao, J. Zhou, Z. Suo, A theory of coupled diffusion and large deformation in polymeric gels, J. Mech. Phys. Solids 56 (2008) 1779–1793.
[19] Q. Liu, H. Li, K.Y. Lam, Development of a multiphysics model to characterize the responsive behavior of magnetic-sensitive hydrogels with finite deformation, J. Phys. Chem. B 121 (2017) 5633–5646.
[20] R. Marcombe, et al., A theory of constrained swelling of a pH-sensitive hydrogel, Soft Matter 6 (2010) 784–793.
[21] K. Takahashi, T. Takigawa, T. Masuda, Swelling and deswelling kinetics of poly (N-isopropylacrylamide) gels, J. Chem. Phys. 120 (2004) 2972–2979.
[22] X. Wang, W. Hong, A visco-poroelastic theory for polymeric gels, Proc. R. Soc. Lond. Ser. A Math. Phys. Eng. Sci. 468 (2012) 3824–3841.
[23] H. Li, S.S. Mulay, 2D simulation of the deformation of pH-sensitive hydrogel by novel strong-form meshless random differential quadrature method, Comput. Mech. 48 (2011) 729–753.
[24] F. Lai, H. Li, Modeling of effect of initial fixed charge density on smart hydrogel response to ionic strength of environmental solution, Soft Matter 6 (2010) 311–320.
[25] N. Bouklas, C.M. Landis, R. Huang, A nonlinear, transient finite element method for coupled solvent diffusion and large deformation of hydrogels, J. Mech. Phys. Solids 79 (2015) 21–43.
[26] Z. Liu, S. Swaddiwudhipong, W. Hong, Pattern formation in plants via instability theory of hydrogels, Soft Matter 9 (2013) 577–587.
[27] Z. Liu, W. Hong, Z. Suo, S. Swaddiwudhipong, Y. Zhang, Modeling and simulation of buckling of polymeric membrane thin film gel, Comput. Mater. Sci. 49 (2010) S60–S64.
[28] W. Hong, Z. Liu, Z. Suo, Inhomogeneous swelling of a gel in equilibrium with a solvent and mechanical load, Int. J. Solids Struct. 46 (2009) 3282–3289.
[29] S.A. Chester, C.V. Di Leo, L. Anand, A finite element implementation of a coupled diffusion-deformation theory for elastomeric gels, Int. J. Solids Struct. 52 (2015) 1–18.
[30] J. Zhang, X. Zhao, Z. Suo, H. Jiang, A finite element method for transient analysis of concurrent large deformation and mass transport in gels, J. Appl. Phys. 105 (2009) 093522.
[31] Z. Duan, J. Zhang, Y. An, H. Jiang, Simulation of the transient behavior of gels based on an analogy between diffusion and heat transfer, J. Appl. Mech. 80 (2013) 041017.
[32] A. Lucantonio, P. Nardinocchi, L. Teresi, Transient analysis of swelling-induced large deformations in polymer gels, J. Mech. Phys. Solids 61 (2013) 205–218.
[33] P. Nardinocchi, A. Lucantonio, L. Teresi, 2012 Comsol Conference. (Comsol, 2012).
[34] X. Zhang, T. Guo, Y. Zhang, Instability analysis of a programmed hydrogel plate under swelling, J. Appl. Phys. 109 (2011) 063527.
[35] T. Tanaka, et al., Mechanical instability of gels at the phase transition, Nature 325 (1987) 796.
[36] B. Li, Y.-P. Cao, X.-Q. Feng, H. Gao, Mechanics of morphological instabilities and surface wrinkling in soft materials: a review, Soft Matter 8 (2012) 5728–5745.
[37] M.K. Kang, R. Huang, Swell-induced surface instability of confined hydrogel layers on substrates, J. Mech. Phys. Solids 58 (2010) 1582–1598.
[38] J.P. Boyd, N. Flyer, Compatibility conditions for time-dependent partial differential equations and the rate of convergence of Chebyshev and Fourier spectral methods, Comput. Methods Appl. Mech. Engrg. 175 (1999) 281–309.
[39] T. Kobayashi, Y. Mihara, Application of artificial damping method to practical instability problems, in: Science in the Age of Experience, 2017.
[40] P. Deuflhard, A modified Newton method for the solution of ill-conditioned systems of nonlinear equations with application to multiple shooting, Numer. Math. 22 (1974) 289–315.
[41] T. Tanaka, Kinetics of phase transition in polymer gels, Physica A 140 (1986) 261–268.
[42] E. Brouzés, E. Farge, Interplay of mechanical deformation and patterned gene expression in developing embryos, Curr. Opin. Genetics Dev. 14 (2004) 367–374.
[43] S.J. DuPont Jr., R.S. Cates, P.G. Stroot, R. Toomey, Swelling-induced instabilities in microscale, surface-confined poly (N-isopropylacryamide) hydrogels, Soft Matter 6 (2010) 3876–3882.
[44] T. Mora, A. Boudaoud, Buckling of swelling gels, Eur. Phys. J. E 20 (2006) 119–124.
[45] H. Lee, J. Zhang, H. Jiang, N.X. Fang, Prescribed pattern transformation in swelling gel tubes by elastic instability, Phys. Rev. Lett. 108 (2012) 214304.
[46] C. Yu, et al., Electronically programmable, reversible shape change in two-and three-dimensional hydrogel structures, Adv. Mater. 25 (2013) 1541–1546.
[47] T.L. Bergman, F.P. Incropera, D.P. DeWitt, A.S. Lavine, Fundamentals of Heat and Mass Transfer, John Wiley & Sons, 2011.
[48] I. Aibara, S. Mukai, S. Hashimoto, Plasmonic-heating-induced nanoscale phase separation of free poly (N-isopropylacrylamide) molecules, J. Phys. Chem. C 120 (2016) 17745–17752.